

## Polarizing Free Electrons in Optical Near Fields

Deng Pan<sup>1,2,\*</sup> and Hongxing Xu<sup>3,2,†</sup><sup>1</sup>State Key Laboratory of Precision Spectroscopy, East China Normal University, Shanghai 200062, China<sup>2</sup>Institute of Quantum Materials and Physics, Henan Academy of Sciences, Zhengzhou 450046, China<sup>3</sup>School of Physics and Technology, Wuhan University, Wuhan 430072, China (Received 18 June 2022; accepted 3 March 2023; published 4 May 2023)

Polarizing electron beams using light is highly desirable but exceedingly challenging, as the approaches proposed in previous studies using free-space light usually require enormous laser intensities. Here, we propose the use of a transverse electric optical near field, extended on nanostructures, to efficiently polarize an adjacent electron beam by exploiting the strong inelastic electron scattering in phase-matched optical near fields. Intriguingly, the two spin components of an unpolarized incident electron beam—parallel and antiparallel to the electric field—are spin-flipped and inelastically scattered to different energy states, providing an analog of the Stern-Gerlach experiment in the energy dimension. Our calculations show that when a dramatically reduced laser intensity of  $\sim 10^{12}$  W/cm<sup>2</sup> and a short interaction length of 16  $\mu$ m are used, an unpolarized incident electron beam interacting with the excited optical near field can produce two spin-polarized electron beams, both exhibiting near unity spin purity and a 6% brightness relative to the input beam. Our findings are important for optical control of free-electron spins, preparation of spin-polarized electron beams, and applications in material science and high-energy physics.

DOI: [10.1103/PhysRevLett.130.186901](https://doi.org/10.1103/PhysRevLett.130.186901)

*Introduction.*—After Stern and Gerlach’s celebrated experiment using inhomogeneous magnetic fields to separate neutral atoms by spin, Bohr and Pauli pointed out that a similar scheme could not be simply applied to polarize charged particles due to the influence of the Lorentz force [1–3]. Consequently, alternative mechanisms are required to prepare spin-polarized electrons [4]. Two main approaches have been implemented experimentally: one uses semiconductor photocathodes with negative electron affinities as electron sources [5–7], while the other is based on spin-dependent radiation from relativistic electron beams in storage rings (i.e., the Sokolov-Ternov effect) [8–10]. Importantly, spin-polarized electron beams have served as an essential tool for investigating the magnetic properties of solid-state materials and molecules [11–13], probing atom and nucleon spin structures [14–16], and studying fundamental problems in high-energy physics [17–19].

Concentrated efforts are now being devoted to exploring the possibility of polarizing electrons using free-space light. In this area, the spin-flip dynamics of electrons are manipulated via Compton scattering [20–25] or by the Kapitza-Dirac effect [26–36], which involve the use of either a single laser beam or two counterpropagating lasers [37–39], respectively. However, since direct photon absorptions or emissions by electrons are forbidden in free space, these free-space phenomena are at least second-order quantum processes, which occur only at enormous laser intensities (typically,  $\sim 10^{18}$ – $10^{22}$  W/cm<sup>2</sup>, depending on the interaction time [40]). Notably, although electron spin flips have been predicted in these free-space approaches,

the scattered electrons of opposite spins overlap considerably in energy and space, severely limiting their usefulness in generating spin-polarized electron beams.

In contrast to these free-space scenarios, interactions between moving electrons and optical near fields are intrinsically inelastic, mediated by large photonic momenta. For example, in Cherenkov radiation (CR) and electron energy-loss spectroscopy (EELS), electron beams spontaneously release photons into vacuum photonic modes. Recently, the photon-induced near-field electron microscopy (PINEM) technique has been intensively investigated [41–61]. Unlike those spontaneous-emission-like phenomena such as CR and EELS, a laser is introduced in PINEM to excite the optical near field of a nanostructure. Surprisingly, recent PINEM experiments [57,58] have observed emissions or absorptions of hundreds of photons by a single electron at moderate laser intensity, by matching the electron velocity and near-field phase velocity. Given such strong inelastic scattering, it is thus illuminating to explore whether electron spins can be efficiently manipulated using optical near fields.

To control electron spins via inelastic scatterings in optical near fields, the spin angular momentum (AM) of an electron must be switched between  $-\hbar/2$  and  $\hbar/2$  by directly absorbing or emitting a photon with an AM of  $\hbar$ . Significantly, optical near fields inherently possess an extraordinary transverse AM [62–64] perpendicular to their propagation directions, leading to new exciting physics such as spin-orbit interactions [65–69], topological photonics phenomena [70–72], unidirectional emissions [73–76], and chiral quantum optics [77–80]. Furthermore, the

symmetry of the evanescent field is reduced compared to the free-space light, which can relax the symmetry requirement [81,82] for quantum spin transitions.

In this Letter, we reveal an efficient pathway for polarizing electron beams via interactions with a transverse electric (TE) optical near field, exploiting the giantly enhanced and chiral electron–near-field interactions. Compared to previous studies that involve only free-space light, the intensity of the laser required to induce pronounced electron spin-flip transitions in our approach is dramatically reduced (to  $\sim 10^{12}$  W/cm<sup>2</sup> in our calculations). More importantly, for an unpolarized incident electron beam, the two spin components along the electric field direction are scattered to different energy states, thereby offering a direct way to prepare spin-polarized electron beams of high purity.

*Model system.*—In this Letter, we investigate a two-dimensional (2D) periodic nanostructure, such as a nanowire array (see Fig. 1) illuminated by a laser. The laser excites an optical near field that induces inelastic and spin-flip scattering of an adjacent electron beam propagating along  $+\hat{z}$ . For simplicity, we assume a 2D electron beam with its  $y$ -component wave vector vanishing [40]. In PINEM, the electric field component parallel to the electron beam dominates, inducing only spin-preserving transitions. To enable spin-flip transitions, we consider a TE configuration (Fig. 1) in which only  $\mathcal{E}_y$  is present. The total electric field includes a near-field component and can be approximated as  $\vec{\mathcal{E}}_y(\mathbf{r}) = \vec{\mathcal{E}}_y^b(x) + [\Delta\vec{\mathcal{E}}_y(x)e^{iq_z z} + \text{c.c.}]$ , where  $q_z = 2\pi/a$ . We also assume a monochromatic light field, i.e.,  $\vec{\mathcal{E}}_y(\mathbf{r}, t) = \vec{\mathcal{E}}_y(\mathbf{r})e^{-i\omega t} + \text{c.c.}$ , which can be extended to a pulsed laser field, as in the PINEM theory [57].

Similar to previous PINEM experiments [57,58], we ensure a strong electron-photon interaction by considering a resonant situation throughout this work. We assume that

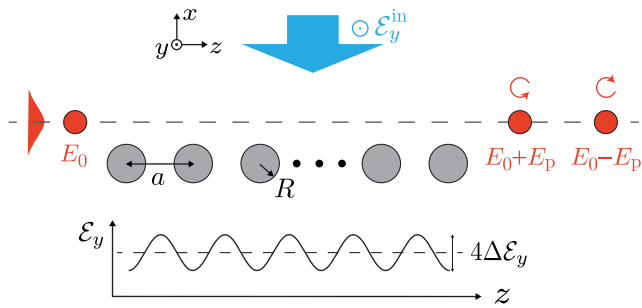


FIG. 1. Illustration of the process of polarizing electrons in an optical near field. A wide TE laser beam (blue arrow) is normally incident on a nanowire array, with the electric field oriented parallel to the nanowires. This produces a near field that is periodically modulated (bottom panel). Unpolarized electrons passing through the optical near field are scattered by either absorbing or emitting a photon of energy  $E_p$ , with the spins of the scattered electrons aligned along  $+\hat{y}$  and  $-\hat{y}$  (red circular arrows), respectively.

the initial electron velocity matches the near-field phase velocity, i.e.,  $\beta = v_0/c = a/\lambda$ , where  $\lambda$  is the vacuum photon wavelength. Unlike the high-energy electron beams ( $> 100$  keV) typically used in PINEM (see exceptions in [61,83]), as we shall explain below, the spin-flip transitions of the electrons are significant only for low-energy electrons. The low-energy electron beam we consider is not as tightly bounded as in PINEM (see red shade in Fig. 1), and the high laser intensity required to achieve significant spin-flip transitions can cause electron-beam reshaping. However, our theory, presented below, can fully capture both the spin dynamics and diffraction effects of electron beams in the optical near field.

*Theory of spin dynamics.*—As the spin-flip effect is significant only for low electron velocities (see below), we restrict this work to nonrelativistic situations and neglect the Coulomb repulsion [40,84]. Given this limit, the spin dynamics of an electron beam is governed by Pauli’s equation,  $(\hat{\mathbf{p}}^2/2m_e + \hat{\mathcal{H}}_I)\Psi(\mathbf{r}, t) = i\hbar\partial_t\Psi(\mathbf{r}, t)$  [ $\mathbf{r} = (x, z)$ ], where the interaction Hamiltonian in the radiation gauge reads

$$\hat{\mathcal{H}}_I = \frac{e}{m_e c} \mathbf{A}(\mathbf{r}, t) \cdot \hat{\mathbf{p}} + \mu_B \mathbf{B}(\mathbf{r}, t) \cdot \vec{\sigma} + \frac{e^2}{2m_e c^2} \mathbf{A}^2(\mathbf{r}, t),$$

$\hat{\mathbf{p}}$  is the momentum operator,  $\mu_B = e\hbar/2m_e c$  is the Bohr magneton, and  $\vec{\sigma} = [\sigma_x, \sigma_y, \sigma_z]$  is the three-vector Pauli matrix. The wave function in Pauli’s equation is described using the two-component spinors,  $\Psi(\mathbf{r}, t) = \sum_{\pm} \Psi^{\pm}(\mathbf{r}, t) \otimes |\pm\rangle$ , where  $|+\rangle = [\cos(\theta/2), \sin(\theta/2)e^{i\phi}]^T$  and  $|-\rangle = [\sin(\theta/2), -\cos(\theta/2)e^{i\phi}]^T$  denote the two possible spins of electrons along the direction implicitly defined by the two polar coordinates  $(\theta, \phi)$ . In the radiation gauge, the vector potential is related to the electric field by  $\mathbf{A}(\mathbf{r}) = -i\vec{\mathcal{E}}(\mathbf{r})/q$ , where  $q = \omega/c$ .

Considering an electron beam of initial energy  $E_0$  interacting with an optical near field, the bare electron energy should spread only among discrete levels, i.e.,  $E_n = E_0 + n\hbar\omega$ . In the case of a paraxial and slowly varying electron beam, we can expand  $\Psi^{\pm}$  using the eigenfunction of  $\hat{\mathbf{p}}^2/2m_e$  as  $\Psi^{\pm}(\mathbf{r}, t) = \sum_n \psi_n^{\pm}(\mathbf{r}) e^{i(p_n z - E_n t)/\hbar}$ , where  $p_n = \sqrt{2m_e E_n} \approx p_0 + n\hbar\omega/v_0$ . Using this expansion, and together with a nonrecoil approximation, Pauli’s equation can be rewritten as a set of coupled equations [40],

$$\left( v_0 \hat{p}_z + \frac{\hat{p}_x^2}{2m_e} \right) \psi_n^s(\mathbf{r}) = - \sum_{n's'} \mathcal{M}_{nn'}^{ss'} \psi_{n'}^{s'}(\mathbf{r}), \quad (1)$$

where the nonzero transition matrix elements for the TE electromagnetic field are

$$\begin{aligned} \mathcal{M}_{n,n-1}^{ss'} &= e^{-i\frac{\omega}{v_0} z} \mu_B \langle s | \mathbf{B}(\mathbf{r}) \cdot \vec{\sigma} | s' \rangle, \\ \mathcal{M}_{nn}^{ss} &= \frac{e^2}{m_e \omega^2} |\mathcal{E}_y(\mathbf{r})|^2, \end{aligned} \quad (2)$$

and their Hermitian conjugates  $\mathcal{M}_{n'n}^{s's} = (\mathcal{M}_{nn'}^{ss'})^*$ . The above matrix elements reveal that the magnetic field can induce both spin-flip and spin-preserving transitions. In addition, the  $\mathbf{A}^2$  term in  $\hat{\mathcal{H}}_I$ , which corresponds to the ponderomotive force, introduces an additional phase to the wave function [85].

As seen from Eq. (2), for the infinitely extended nanostructure shown in Fig. 1, resonantly enhanced interactions arise when  $\omega/v_0 = q_z$  or equivalently  $v_0/c = a/\lambda$  [57,58]. Furthermore, only the near-field component propagating parallel to the electron beam, such as the electric field component  $\Delta\vec{\mathcal{E}}_y(x)e^{iq_z z}$ , contributes to the electron scatterings. Assuming that the electron beam is above the nanowires (see Fig. 1), this evanescent near field is characterized by a factor  $e^{-q_x x}$ , and the corresponding magnetic field according to Maxwell's equations is  $\Delta\mathbf{B}(\mathbf{r}) = \mathbf{q} \times \Delta\vec{\mathcal{E}}_y(x)e^{iq_z z}/q$ , where  $q_x = \sqrt{q_z^2 - q^2}$  and  $\mathbf{q} = (iq_x, 0, q_z)$ . Using  $\Delta\mathbf{B}(\mathbf{r})$ , we can simplify the off-diagonal matrix elements in Eq. (2) to

$$\mathcal{M}_{n,n-1}^{ss'} = \mu_B [\langle s | (\mathbf{q} \times \hat{y}) \cdot \vec{\sigma} | s' \rangle] \Delta\mathcal{E}_y(x)/q. \quad (3)$$

It is important to note that  $\Delta\mathbf{B}(\mathbf{r})$  is circularly polarized along  $+\hat{y}$  when  $q_z \gg q$ , which is associated with the transverse spin AM in the evanescent near field [62–64]. This transverse near-field AM results in chiral interactions with the electron spins in the same direction. More precisely, if  $|\pm\rangle$  is defined along  $\pm\hat{y}$ , we have  $\mathcal{M}_{n,n-1}^{+-} \approx 2i\mu_B\Delta\mathcal{E}_y\beta^{-1}$  while  $\mathcal{M}_{n,n-1}^{-+} \approx 0$ . By contrast, for electron spins in the  $x$ - $z$  plane, which is perpendicular to the near-field AM, the chiral symmetry is preserved.

Assuming an incident spin along  $+\hat{y}$ , in the weak-interaction regime  $|\psi_0^+(z) \approx 1|$ , the spin-flip transition probabilities over a propagation distance of  $L$  can be evaluated, according to Eqs. (1) and (3), by  $P_{\text{flip}} \approx \sum_{\pm} |\mathcal{M}_{\pm 1,0}^{\mp+} L/v_0\hbar|^2 \approx |2\mu_B\Delta\mathcal{E}_y L/c\hbar|^2 \beta^{-4}$ , which is greatly enhanced when electrons slow down. However, an excessively small electron velocity widens the electron beam waist and requires a more localized near field ( $\sim e^{-q_x x}$ ) to fulfill the phase-match condition, thereby reducing the chance of electron-photon interaction. Consequently, we assume a moderate electron velocity, i.e.,  $\beta = 1/10$ , in the detailed calculations below.

*Diffractionless approximation.*—To concisely reveal the spin dynamics of an electron beam in optical near fields, we begin by using the diffractionless approximation ( $\hat{p}_x^2 \approx 0$ ) and assuming that the electron dynamics on different straight trajectories ( $x = \text{const}$ ) are independent. This approximation simplifies the electron spin dynamics governed by Eq. (1) to a one-dimensional (1D) equation. The numerical results calculated by the reduced 1D equation are presented in Fig. 2, where we adopt the simplified matrix elements in Eq. (3) and consider spin-polarized incident

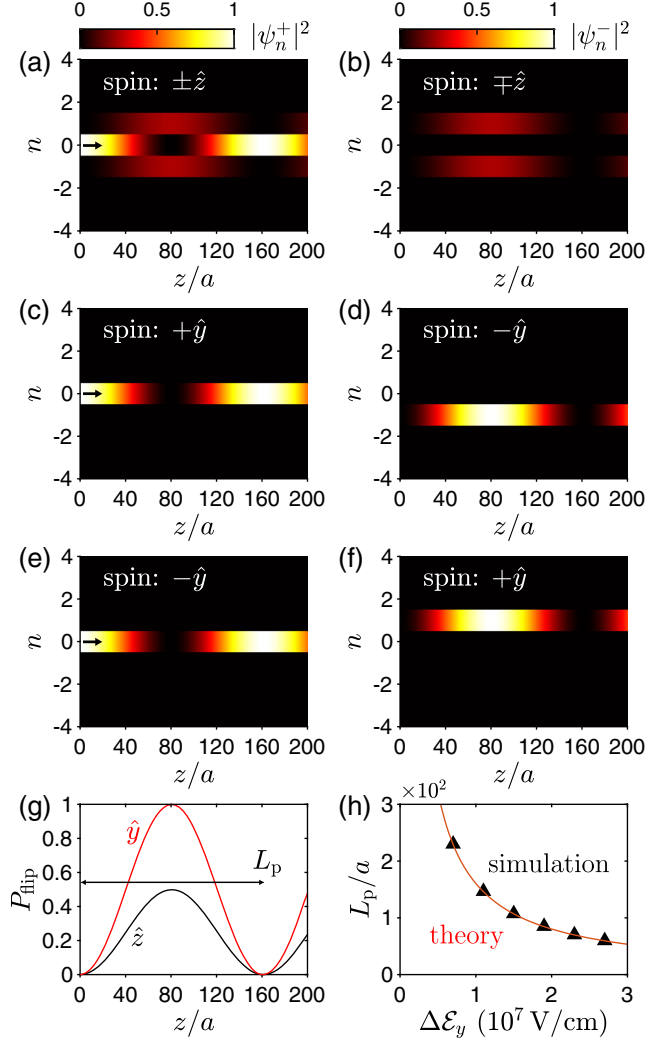


FIG. 2. (a)–(f) Distributions of the (a),(c),(e) spin-preserving ( $|\psi_n^+|^2$ ) and (b),(d),(f) spin-flipped electrons ( $|\psi_n^-|^2$ ) among discrete energy levels (plotted in the color scale as ribbons) for different propagation distances, calculated within the diffractionless approximation ( $x = \text{const}$ ). The input electron beams are spin-up polarized (see black arrows, i.e.,  $\psi_0^+$ ) along (a)  $\pm\hat{z}$ , (c)  $+\hat{y}$ , and (e)  $-\hat{y}$ , respectively. (g) The spin-flip probabilities for incident electron spins along  $\hat{z}$  and  $\hat{y}$  show the same period of  $L_p$ . (h) The period  $L_p$  for different  $\Delta\mathcal{E}_y$  (see definition in Fig. 1). We assume an electric field component  $\Delta\mathcal{E}_y = 1 \times 10^7$  V/cm in (a)–(g), and use parameters  $\lambda = 1 \mu\text{m}$  and  $a = 100$  nm for all calculations.

electron beams. The incident spin directions [see Figs. 2(a), 2(c), 2(e)] are consistently denoted as “spin-up” ( $s = +$ ).

Because of the circular polarization of  $\Delta\mathbf{B}$ , the electron spin dynamics in the  $x$ - $z$  plane is isotropic. Here, we chose the incident electron spin  $\hat{s}_{\text{in}} = \pm\hat{z}$  to demonstrate the electron spin dynamics in the  $x$ - $z$  plane [40] [Figs. 2(a) and 2(b)]. As the electron interacts with the near field, the initial state occupancy,  $|\psi_0^+(z=0)|^2 = 1$ , gradually decreases [Fig. 2(a)], while the adjacent energy levels  $\psi_{\pm 1}^{\pm}$  of both

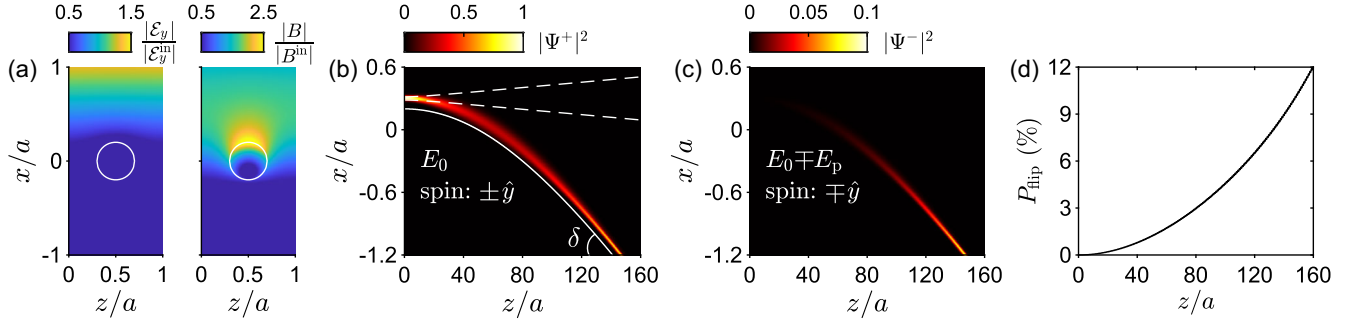


FIG. 3. (a) Electric (right) and magnetic (left) near field surrounding a nanowire array excited by a plane wave of wavelength  $\lambda = 1 \mu\text{m}$  ( $E_p = 1.24 \text{ eV}$ ). We assume a platinum nanowire array, with an experimentally measured optical permittivity  $-105.76 + 16.49i$  [86] for the chosen photon energy, radius of  $R = 20 \text{ nm}$ , and a lattice constant of  $a = 100 \text{ nm}$ . (b)–(d) The spatial distributions of the (b) spin-preserving and (c) spin-flipped electron density, and the (d) spin-flip probability, calculated for an electron beam interacting with the optical near field shown in (a). An electron beam, spin-polarized along  $\pm\hat{y}$  and with a phase-matched velocity, i.e.,  $\beta = 1/10$ , is initially focused at  $z = 0$  and  $x = 0.3a$ , with a waist of  $3 \text{ nm}$ . In (c), the spin-flipped electrons are scattered to the state of energy  $E_p \mp E_0$ . The unperturbed beam width is shown by the white dashed curves in (b). The electron beam is slightly deflected due to a reshaping effect in the optical field, and the nanowire array is adaptively rearranged to avoid crossing (the top of the nanowires are shown by the white solid curve). The incident electric field is assumed to be  $\mathcal{E}_y^{\text{in}} = 4 \times 10^7 \text{ V/cm}$ .

spin directions are equally populated via inelastic scattering. The populations undergo oscillations upon further propagation. The populations are symmetric in energy and equal for incident spins along  $+\hat{z}$  and  $-\hat{z}$ , which are rooted in the lack of a chiral symmetry-breaking mechanism as described by Eq. (3). This equality ultimately suggests that it is impossible to separate the two spin components in the  $x$ - $z$  plane of incident unpolarized electron beams.

In contrast, when incident electron spins are parallel to the near-field AM, the electrons chirally couple to the field, resulting in asymmetric patterns of the energy state populations [Figs. 2(c)–2(f)]. For  $\hat{s}_{\text{in}} = +\hat{y}$ , the only possible transition from the initial state is that the electron simultaneously releases an energy quantum of  $\hbar\omega$  and an AM quantum of  $\hbar$  into the near field, namely,  $\psi_0^+ \rightarrow \psi_{-1}^-$  [Figs. 2(c) and 2(d)]. Likewise,  $\hat{s}_{\text{in}} = -\hat{y}$  only gives rise to the transition  $\psi_0^+ \rightarrow \psi_{+1}^-$  [Figs. 2(e) and 2(f)]. However, emissions or absorptions of multiple quanta of photon AM by one electron are not allowed, so only the three energy levels,  $\psi_0^+$  and  $\psi_{\pm 1}^-$ , are populated in Figs. 2(a)–2(f), in contrast to the random walk [60] pattern observed in PINEM. Considering an unpolarized incident electron beam, the electrons scattered to states of energy  $E_{+1}$  and  $E_{-1}$  are spin polarized along  $+\hat{y}$  or  $-\hat{y}$ , respectively, and can be further separated by an energy filter. This offers a pathway for polarizing electron beams in a mixed state. Importantly, our approach can theoretically achieve a spin purity of unity for the polarized electron beams, and this purity is not expected to significantly deteriorate under realistic experimental conditions, as suggested by PINEM experiments.

The spin-flip probabilities [Fig. 2(g)], defined as  $P_{\text{flip}} = |\Psi^-|^2/|\Psi|^2$ , also exhibit oscillatory behaviors, which can be captured by  $P_{\text{flip}} = P_{\text{flip}}^{\text{max}} \sin^2(\pi z/L_p)$ , where  $P_{\text{flip}}^{\text{max}} = 0.5$  and  $1$  for incident spins along the  $z$  and  $y$

directions, respectively. The repetition of the population observed here is, in fact, a Rabi oscillation among the two relevant electron states, e.g.,  $\psi_0^+$  and  $\psi_{-1}^-$  for  $\hat{s}_{\text{in}} = +\hat{y}$ , induced by the interactions described in Eq. (3). The corresponding Rabi frequency can be found as  $\Omega_R = 2|\mathcal{M}_{-1,0}^-|/\hbar = 4\mu_B\Delta\mathcal{E}_y/\beta\hbar$ , which leads to a period of  $L_p = 2\pi v_0/\Omega_R$  that is consistent with the numerical results [Fig. 2(h)]. Notably, within the diffractionless approximation, Fig. 2 is a universal plot, which is scaled only by the dimensionless factor of  $z/L_p$ .

*Spin-flip of diffractive electron beams.*—To include the diffraction effects, we perform 2D calculations of Eq. (1), incorporating both the transverse momentum (the  $\hat{p}_x^2$  term) and the pondermotive force. Our calculations utilize a numerically solved electromagnetic field [see Fig. 3(a)], where  $\mathbf{B}$  is enhanced near the nanowire. We consider a Gaussian electron beam, which is spin-polarized along  $\pm\hat{y}$  and propagates through the near-field calculated above. The beam is focused at  $z = 0$  with a distribution of  $\Psi(x, z = 0) = \sqrt{2/\pi w_0^2} e^{-(x-30[\text{nm}])^2/w_0^2}$ , where  $w_0 = 3 \text{ nm}$  is the beam waist. The unperturbed Gaussian beam width,  $w(z) = w_0 \sqrt{1 + (z/z_R)^2}$ , is indicated by the dashed curves in Fig. 3(b), where  $z_R = \pi w_0^2/\lambda_e$  and  $\lambda_e = 2\pi\hbar/p_0$  is the electron wavelength.

During interactions with the near field, the Gaussian electron beam is reshaped due to an additional phase imprinted by the pondermotive force (see, e.g., [85]). For the TE field considered in this work, the pondermotive force introduces a phase, captured by  $d\phi = \mathcal{M}_{nn}^{ss} dz/\hbar v_0$ , according to Eq. (1). Consequently, the electron wave segment propagating in a region of higher intensity accumulates a larger phase, causing the electron beam to be deflected toward the nanowires surrounded by lower field intensity [see  $|\mathcal{E}_y|$  in Fig. 3(a)].

To avoid crossing of the electron beam with the nanowires, as shown by the solid curve of  $x_j + R$  in Fig. 3(b), we adaptively displace each nanowire slightly in the  $x$  direction, while maintaining the distance between the center of each nanowire,  $(x_j, z_j)$  ( $j$ th nanowire), and the electron-density peak in the plane  $z = z_j$ . With this adaptive design, the electron beam experiences almost constant acceleration along the  $x$  direction, following a paraboliclike trajectory [40]. Additionally, the reshaping effect leads to a better confinement and even refocusing of the electron beam. We note that the paraxial approximation assumed to derive Eq. (1) is valid, since the electron beam deflection angle,  $\delta \approx 1.8a/120a \approx 15$  mrad [see Fig. 3(b)], is still small.

Despite the reshaping effect, our adaptive design of the nanowire array ensures a strong interaction between the electron beam and the magnetic field localized around the nanowire [see  $|\mathbf{B}|$  in Fig. 3(a)], which results in efficient spin-flip transitions. As shown in Figs. 3(c) and 3(d), the population of spin-flipped electrons with energy  $E_0 \mp E_p$  continuously increases along the propagation, and the spin-flip probability  $P_{\text{flip}}$  reaches  $\sim 12\%$  at a propagation distance of 16  $\mu\text{m}$ . A comparable estimate of  $P_{\text{flip}}$  ( $\sim 15\%$ ) can be found using the scaling law shown in Fig. 2(g), with the modulated electric field component of  $\Delta\mathcal{E}_y \approx 0.032\mathcal{E}_y^{\text{in}}$  obtained from Fig. 3(a). Under the same parameters as in Fig. 3, an unpolarized incident electron beam can produce two electron beams spin polarized along  $\pm\hat{y}$  and with energies of  $E_0 \pm E_p$ . Both beams exhibit high spin purity and a 6% brightness relative to the input beam.

*Concluding remarks.*—In this Letter, we propose an exceptionally efficient mechanism to polarize electrons using optical near fields. Our method is also applicable to the important category of electron vortex beams [87,88], since spin and orbital AM are decoupled in paraxial beams. By superposing TE and TM components properly, the near-field AM can be oriented in any direction [63], and the interplay with the PINEM scattering may lead to new opportunities for electron manipulation. The electron beams produced using our approach comprise coherent superpositions of states with different AM, energies and spins, which could lead to novel beam dynamics [89–92]. The spin-flip effect proposed in the present work is feasible, because PINEM is already a well-established technology that has even been implemented using a scanning electron microscope [61]. The incident laser intensity adopted in Fig. 3,  $I^{\text{in}} = 8.5 \times 10^{12}$  W/cm<sup>2</sup>, is attainable using commercial ultrafast lasers, and the intensity  $I^{\text{in}}$  required to achieve the same  $P_{\text{flip}}$  as in Fig. 3 can be further reduced by extending the interaction length. As the typical laser damage threshold of metals is several J/cm<sup>2</sup> and the plasmon-enhanced absorption is absent for the TE illumination, the nanostructures should sustain a laser illumination with a pulse duration of  $\sim 10^2$  fs, provided

the peak intensity of  $I^{\text{in}} = 8.5 \times 10^{12}$  W/cm<sup>2</sup>. In addition, the use of a higher input electric current can further reduce the laser intensity required to induce observable spin-flipped electrons and prove the spin-flip effect proposed in this Letter.

This work has been supported in part by the Ministry of Science and Technology of China (Grant No. 2021YFA1401100) and the National Natural Science Foundation of China (NSFC, Grants No. 12274135, and No. 12004117). The authors thank Yanfei Li and Sven Ahrens for helpful discussions.

\*Corresponding author.

dpan@lps.ecnu.edu.cn

†Corresponding author.

hxxu@whu.edu.cn

- [1] W. Pauli, in *Proceedings of the Sixth Solvay Conference, 1930* (Gauthier-Villars, Brussels, 1932).
- [2] H. Batelaan, T. J. Gay, and J. J. Schwendiman, *Phys. Rev. Lett.* **79**, 4517 (1997).
- [3] G. H. Rutherford and R. Grobe, *Phys. Rev. Lett.* **81**, 4772 (1998).
- [4] J. Kessler, *Polarized Electrons* (Springer Science & Business Media, New York, 1985), Vol. 1.
- [5] D. T. Pierce, F. Meier, and P. Zürcher, *Appl. Phys. Lett.* **26**, 670 (1975).
- [6] D. T. Pierce and F. Meier, *Phys. Rev. B* **13**, 5484 (1976).
- [7] D. T. Pierce, R. Celotta, G.-C. Wang, W. Unertl, A. Galejs, C. Kuyatt, and S. Mielczarek, *Rev. Sci. Instrum.* **51**, 478 (1980).
- [8] A. A. Sokolov and M. Ternov, *Sov. Phys. Dokl.* **8**, 1203 (1964).
- [9] A. A. Sokolov and I. M. Ternov, *Sov. Phys. J.* **10**, 39 (1967).
- [10] V. A. Bordovitsyn *et al.*, *Synchrotron Radiation Theory and its Development: In Memory of I M Ternov* (World Scientific, Singapore, 1999), Vol. 5.
- [11] R. Feder, *Polarized Electrons in Surface Physics* (World Scientific, Singapore, 1986), Vol. 1.
- [12] J. Kirschner, *Polarized Electrons at Surfaces, Springer Tracts in Modern Physics* (Springer, Berlin, 1985).
- [13] M. Getzlaff, *Surface Magnetism: Correlation of Structural, Electronic and Chemical Properties with Magnetic Behavior* (Springer Science & Business Media, New York, 2010), Vol. 240.
- [14] X. Ji, *Phys. Rev. Lett.* **78**, 610 (1997).
- [15] T. J. Gay, *Adv. At. Mol. Opt. Phys.* **57**, 157 (2009).
- [16] C. A. Aidala, S. D. Bass, D. Hasch, and G. K. Mallot, *Rev. Mod. Phys.* **85**, 655 (2013).
- [17] C. Y. Prescott, W. Atwood, R. Cottrell, H. Destaeblér, E. L. Garwin, A. Gonidec, R. H. Miller, L. Rochester, T. Sato, D. Sherden *et al.*, *Phys. Lett.* **77B**, 347 (1978).
- [18] P. Anthony, R. Arnold, C. Arroyo, K. Baird, K. Bega, J. Biesiada, P. Bosted, M. Breuer, R. Carr, G. Cates *et al.*, *Phys. Rev. Lett.* **92**, 181602 (2004).
- [19] A. Accardi, J. Albacete, M. Anselmino, N. Armesto, E. Aschenauer, A. Bacchetta, D. Boer, W. Brooks, T. Burton, N.-B. Chang *et al.*, *Eur. Phys. J. A* **52**, 268 (2016).

- [20] M. W. Walser, D. J. Urbach, K. Z. Hatsagortsyan, S. X. Hu, and C. H. Keitel, *Phys. Rev. A* **65**, 043410 (2002).
- [21] D. Del Sorbo, D. Seipt, T. G. Blackburn, A. G. R. Thomas, C. D. Murphy, J. G. Kirk, and C. P. Ridgers, *Phys. Rev. A* **96**, 043407 (2017).
- [22] D. Seipt, D. Del Sorbo, C. P. Ridgers, and A. G. R. Thomas, *Phys. Rev. A* **98**, 023417 (2018).
- [23] Y.-F. Li, R. Shaisultanov, K. Z. Hatsagortsyan, F. Wan, C. H. Keitel, and J.-X. Li, *Phys. Rev. Lett.* **122**, 154801 (2019).
- [24] H.-H. Song, W.-M. Wang, J.-X. Li, Y.-F. Li, and Y.-T. Li, *Phys. Rev. A* **100**, 033407 (2019).
- [25] Y.-F. Li, Y.-Y. Chen, K. Z. Hatsagortsyan, and C. H. Keitel, *Phys. Rev. Lett.* **128**, 174801 (2022).
- [26] D. Freimund and H. Batelaan, *Laser Phys.* **13**, 892 (2003).
- [27] L. Rosenberg, *Phys. Rev. A* **70**, 023401 (2004).
- [28] S. Ahrens, H. Bauke, C. H. Keitel, and C. Müller, *Phys. Rev. Lett.* **109**, 043601 (2012).
- [29] S. Ahrens, H. Bauke, C. H. Keitel, and C. Müller, *Phys. Rev. A* **88**, 012115 (2013).
- [30] S. McGregor, W. C.-W. Huang, B. A. Shadwick, and H. Batelaan, *Phys. Rev. A* **92**, 023834 (2015).
- [31] M. M. Dellweg, H. M. Awwad, and C. Müller, *Phys. Rev. A* **94**, 022122 (2016).
- [32] M. M. Dellweg and C. Müller, *Phys. Rev. Lett.* **118**, 070403 (2017).
- [33] S. Ahrens, *Phys. Rev. A* **96**, 052132 (2017).
- [34] A. Ebadati, M. Vafaei, and B. Shokri, *Phys. Rev. A* **98**, 032505 (2018).
- [35] S. Ahrens, Z. Liang, T. Čadež, and B. Shen, *Phys. Rev. A* **102**, 033106 (2020).
- [36] S. Ahrens, Z. Guan, and B. Shen, *Phys. Rev. A* **105**, 053123 (2022).
- [37] P. L. Kapitza and P. A. M. Dirac, *Proc. Cambridge Philos. Soc.* **29**, 297 (1933).
- [38] H. Batelaan, *Rev. Mod. Phys.* **79**, 929 (2007).
- [39] D. L. Freimund, K. Aflatooni, and H. Batelaan, *Nature (London)* **413**, 142 (2001).
- [40] See Supplemental Material at <http://link.aps.org/supplemental/10.1103/PhysRevLett.130.186901> for a derivation of Eq. (1), comparisons of the spin-flip efficiency with those of previous studies, evaluation of the impact of using 3D electron beams, assessment of Coulomb repulsion, estimation of the parabolic arrangement of nanowires, and other additional calculations.
- [41] B. Barwick, D. J. Flannigan, and A. H. Zewail, *Nature (London)* **462**, 902 (2009).
- [42] F. J. García de Abajo, A. Asenjo Garcia, and M. Kociak, *Nano Lett.* **10**, 1859 (2010).
- [43] S. T. Park, M. Lin, and A. H. Zewail, *New J. Phys.* **12**, 123028 (2010).
- [44] S. T. Park and A. H. Zewail, *J. Phys. Chem. A* **116**, 11128 (2012).
- [45] F. O. Kirchner, A. Gliserin, F. Krausz, and P. Baum, *Nat. Photonics* **8**, 52 (2014).
- [46] L. Piazza, T. T. A. Lummen, E. Quiñonez, Y. Murooka, B. Reed, B. Barwick, and F. Carbone, *Nat. Commun.* **6**, 6407 (2015).
- [47] A. Feist, K. E. Echternkamp, J. Schauss, S. V. Yalunin, S. Schäfer, and C. Ropers, *Nature (London)* **521**, 200 (2015).
- [48] T. T. A. Lummen, R. J. Lamb, G. Berruto, T. LaGrange, L. D. Negro, F. J. García de Abajo, D. McGrouther, B. Barwick, and F. Carbone, *Nat. Commun.* **7**, 13156 (2016).
- [49] K. E. Echternkamp, A. Feist, S. Schäfer, and C. Ropers, *Nat. Phys.* **12**, 1000 (2016).
- [50] G. M. Vanacore, A. W. P. Fitzpatrick, and A. H. Zewail, *Nano Today* **11**, 228 (2016).
- [51] M. Kozák, J. McNeur, K. J. Leedle, H. Deng, N. Schönenberger, A. Ruehl, I. Hartl, J. S. Harris, R. L. Byer, and P. Hommelhoff, *Nat. Commun.* **8**, 14342 (2017).
- [52] A. Feist, N. Bach, T. D. N. Rubiano da Silva, M. M. Müller, K. E. Priebe, T. Domröse, J. G. Gatzmann, S. Rost, J. Schauss, S. Strauch *et al.*, *Ultramicroscopy* **176**, 63 (2017).
- [53] K. E. Priebe, C. Rathje, S. V. Yalunin, T. Hohage, A. Feist, S. Schäfer, and C. Ropers, *Nat. Photonics* **11**, 793 (2017).
- [54] A. Ryabov and P. Baum, *Science* **353**, 374 (2016).
- [55] Y. Morimoto and P. Baum, *Phys. Rev. A* **97**, 033815 (2018).
- [56] G. M. Vanacore, I. Madan, G. Berruto, K. Wang, E. Pomarico, R. J. Lamb, D. McGrouther, I. Kaminer, B. Barwick, F. J. García de Abajo *et al.*, *Nat. Commun.* **9**, 2694 (2018).
- [57] R. Dahan, S. Nehemia, M. Shentcis, O. Reinhardt, Y. Adiv, X. Shi, O. Be'er, M. H. Lynch, Y. Kurman, K. Wang *et al.*, *Nat. Phys.* **16**, 1123 (2020).
- [58] O. Kfir, H. Lourenço-Martins, G. Storeck, M. Sivis, T. R. Harvey, T. J. Kippenberg, A. Feist, and C. Ropers, *Nature (London)* **582**, 46 (2020).
- [59] K. Wang, R. Dahan, M. Shentcis, Y. Kauffmann, A. Ben Hayun, O. Reinhardt, S. Tsesses, and I. Kaminer, *Nature (London)* **582**, 50 (2020).
- [60] R. Dahan, A. Gorlach, U. Haeusler, A. Karnieli, O. Eyal, P. Yousefi, M. Segev, A. Arie, G. Eisenstein, P. Hommelhoff *et al.*, *Science* **373**, eabj7128 (2021).
- [61] R. Shiloh, T. Chlouba, and P. Hommelhoff, *Phys. Rev. Lett.* **128**, 235301 (2022).
- [62] K. Y. Bliokh, A. Y. Bekshaev, and F. Nori, *Nat. Commun.* **5**, 3300 (2014).
- [63] K. Y. Bliokh and F. Nori, *Phys. Rep.* **592**, 1 (2015).
- [64] J. Eismann, L. Nicholls, D. Roth, M. A. Alonso, P. Banzer, F. Rodríguez-Fortuño, A. Zayats, F. Nori, and K. Bliokh, *Nat. Photonics* **15**, 156 (2021).
- [65] F. J. Rodríguez-Fortuño, G. Marino, P. Ginzburg, D. O'Connor, A. Martínez, G. A. Wurtz, and A. V. Zayats, *Science* **340**, 328 (2013).
- [66] J. Petersen, J. Volz, and A. Rauschenbeutel, *Science* **346**, 67 (2014).
- [67] K. Y. Bliokh, F. J. Rodríguez-Fortuño, F. Nori, and A. V. Zayats, *Nat. Photonics* **9**, 796 (2015).
- [68] F. Cardano and L. Marrucci, *Nat. Photonics* **9**, 776 (2015).
- [69] D. Pan, H. Wei, L. Gao, and H. Xu, *Phys. Rev. Lett.* **117**, 166803 (2016).
- [70] K. Y. Bliokh, D. Smirnova, and F. Nori, *Science* **348**, 1448 (2015).
- [71] K. Y. Bliokh, D. Leykam, M. Lein, and F. Nori, *Nat. Commun.* **10**, 580 (2019).
- [72] T. Ozawa, H. M. Price, A. Amo, N. Goldman, M. Hafezi, L. Lu, M. C. Rechtsman, D. Schuster, J. Simon, O. Zilberberg *et al.*, *Rev. Mod. Phys.* **91**, 015006 (2019).
- [73] R. Mitsch, C. Sayrin, B. Albrecht, P. Schneeweiss, and A. Rauschenbeutel, *Nat. Commun.* **5**, 5713 (2014).

- [74] B. Le Feber, N. Rotenberg, and L. Kuipers, *Nat. Commun.* **6**, 6695 (2015).
- [75] S.-H. Gong, F. Alpegiani, B. Sciacca, E. C. Garnett, and L. Kuipers, *Science* **359**, 443 (2018).
- [76] Y. Chen, S. Qian, K. Wang, X. Xing, A. Wee, K. P. Loh, B. Wang, D. Wu, J. Chu, A. Alu *et al.*, *Nat. Nanotechnol.* **17**, 1178 (2022).
- [77] P. Tighineanu, M. L. Andersen, A. S. Sørensen, S. Stobbe, and P. Lodahl, *Phys. Rev. Lett.* **113**, 043601 (2014).
- [78] S. Mahmoodian, P. Lodahl, and A. S. Sørensen, *Phys. Rev. Lett.* **117**, 240501 (2016).
- [79] P. Lodahl, S. Mahmoodian, S. Stobbe, A. Rauschenbeutel, P. Schneeweiss, J. Volz, H. Pichler, and P. Zoller, *Nature (London)* **541**, 473 (2017).
- [80] S. Barik, A. Karasahin, C. Flower, T. Cai, H. Miyake, W. DeGottardi, M. Hafezi, and E. Waks, *Science* **359**, 666 (2018).
- [81] C. Ospelkaus, U. Warring, Y. Colombe, K. Brown, J. Amini, D. Leibfried, and D. J. Wineland, *Nature (London)* **476**, 181 (2011).
- [82] T. P. Harty, M. A. Sepiol, D. T. C. Allcock, C. J. Ballance, J. E. Tarlton, and D. M. Lucas, *Phys. Rev. Lett.* **117**, 140501 (2016).
- [83] N. Talebi, *Phys. Rev. Lett.* **125**, 080401 (2020).
- [84] M. Mutzafi, I. Kaminer, G. Harari, and M. Segev, *Nat. Commun.* **8**, 650 (2017).
- [85] F. J. García de Abajo and A. Konecna, *Phys. Rev. Lett.* **126**, 123901 (2021).
- [86] W. S. Werner, K. Glantschnig, and C. Ambrosch-Draxl, *J. Phys. Chem. Ref. Data* **38**, 1013 (2009).
- [87] K. Y. Bliokh, Y. P. Bliokh, S. Savel'ev, and F. Nori, *Phys. Rev. Lett.* **99**, 190404 (2007).
- [88] K. Y. Bliokh, I. P. Ivanov, G. Guzzinati, L. Clark, R. Van Boxem, A. Béché, R. Juchtmans, M. A. Alonso, P. Schattschneider, F. Nori *et al.*, *Phys. Rep.* **690**, 1 (2017).
- [89] K. Y. Bliokh, P. Schattschneider, J. Verbeeck, and F. Nori, *Phys. Rev. X* **2**, 041011 (2012).
- [90] K. Y. Bliokh and F. Nori, *Phys. Rev. A* **86**, 033824 (2012).
- [91] G. Guzzinati, P. Schattschneider, K. Y. Bliokh, F. Nori, and J. Verbeeck, *Phys. Rev. Lett.* **110**, 093601 (2013).
- [92] P. Schattschneider, T. Schachinger, M. Stöger-Pollach, S. Löffler, A. Steiger-Thirsfeld, K. Y. Bliokh, and F. Nori, *Nat. Commun.* **5**, 4586 (2014).